

Automated detection of calcified plaque using higher-order spectra cumulant technique in computer tomography angiography images

Original

Automated detection of calcified plaque using higher-order spectra cumulant technique in computer tomography angiography images / Acharya, U. R.; Meiburger, K. M.; Koh, J. E. W.; Ciaccio, E. J.; Vicnesh, J.; Tan, S. K.; Wong, J. H. D.; Aman, R. R. A. R.; Ng, K. H.. - In: INTERNATIONAL JOURNAL OF IMAGING SYSTEMS AND TECHNOLOGY. - ISSN 0899-9457. - 30:2(2020), pp. 285-297. [10.1002/ima.22369]

Availability:

This version is available at: 11583/2860144 since: 2021-01-26T17:00:29Z

Publisher:

John Wiley and Sons Inc.

Published

DOI:10.1002/ima.22369

Terms of use:

This article is made available under terms and conditions as specified in the corresponding bibliographic description in the repository

Publisher copyright

Wiley postprint/Author's Accepted Manuscript

This is the peer reviewed version of the above quoted article, which has been published in final form at <http://dx.doi.org/10.1002/ima.22369>. This article may be used for non-commercial purposes in accordance with Wiley Terms and Conditions for Use of Self-Archived Versions.

(Article begins on next page)



**Automated detection of calcified plaque using higher-order
spectrum cumulant technique in CTA images**

| | |
|-------------------------------|--|
| Journal: | <i>International Journal of Imaging Systems and Technology</i> |
| Manuscript ID | Draft |
| Wiley - Manuscript type: | Research Article |
| Date Submitted by the Author: | n/a |
| Complete List of Authors: | Acharya U, Rajendra; Ngee Ann Polytechnic Meiburger, Kristen Koh, Joel E. W.; Ngee Ann Polytechnic Ciaccio, Edward Vicnesh, Jahmunah Keow, Tan Sock Wong, Jeannie Azmal, Raja Rizal Hoong, Ng Kwan |
| Keywords: | Automated detection, CAD, CTA, higher-order spectrum cumulants |
| | |

SCHOLARONE™
Manuscripts

Automated detection of calcified plaque using higher-order spectrum cumulant technique in CTA images

U Rajendra Acharya^{1,2,3}, Kristen M. Meiburger⁴, Joel En Wei Koh¹, Edward J Ciaccio⁵, Jahmunah Vicnesh¹, Sock Keow Tan^{6,7}, Jeannie Hsiu Ding Wong^{6,7}, Raja Rizal Azman Raja Aman^{6,7}, Kwan Hoong Ng^{6,7}

¹Department of Electronics and Computer Engineering, Ngee Ann Polytechnic, Singapore.

²Department of Biomedical Engineering, School of Science and Technology, Singapore University of Social Sciences, Singapore.

³School of Medicine, Faculty of Health and Medical Sciences, Taylor's University, Subang Jaya, Malaysia.

⁴Department of Electronics and Telecommunications, Politecnico di Torino, Italy.

⁵Department of Medicine, Columbia University, New York, USA.

⁶Department of Biomedical Imaging, Faculty of Medicine, University of Malaya, 50603 Kuala Lumpur, Malaysia.

⁷University of Malaya Research Imaging Centre (UMRIC), Faculty of Medicine, University of Malaya, 50603 Kuala Lumpur, Malaysia.

Abstract

Cardiovascular diseases continue to be the leading cause of death globally and are often associated with atherosclerosis, which can trigger substantial variations in the coronary arteries, possibly causing coronary artery disease (CAD). Coronary artery calcification is known to be a strong and independent forecaster of CAD. Hence coronary computer tomography angiography (CTA) has become a fundamental non-invasive imaging tool to characterize coronary artery plaques. In this paper, an automated algorithm is presented to uncover the presence of a calcified plaque, using 2060 CTA images acquired from 60 patients. Higher-order spectrum cumulants were extracted from each image, thereby providing 2448 descriptive features per image. The features were then reduced using numerous well-established techniques, and ranked according to t-value. Subsequently, the reduced features were input to several classification methods, to achieve the best diagnostic accuracy with a minimum number of features. Optimal results were obtained using the SVM(Support Vector Machine) with a radial basis function, having 22 features obtained with the Multiple Factor Analysis

1
2
3 feature reduction algorithm. The accuracy, positive predictive value, sensitivity, and specificity
4 obtained were 95.83%, 97.05%, 94.54% and 97.13%, respectively. Based on these results, the
5 technique could be useful to automatically and accurately identify calcified plaque evident in CTA
6 images, and may therefore become an important tool to help reduce procedural costs and patient
7 radiation dose.
8
9
10
11
12

13 14 **1. Introduction**

15
16
17
18 Cardiovascular disease (CVD) is a main factor contributing to mortality worldwide, and it is
19 frequently associated with atherosclerosis, which is brought upon by lipoprotein storage,
20 calcification, muscle cell proliferation, inflammation, necrosis, apoptosis, and fibrosis in the
21 arterial wall [1]. The development of atherosclerosis triggers important variations in the
22 coronary blood vessels, often leading to coronary artery disease (CAD) [1].
23
24
25
26
27
28

29
30 In recent years, coronary computer tomography angiography (CTA) has become important
31 for identifying coronary artery stenosis amongst patients suspected to have CAD [2]. Its
32 counterpart, invasive coronary angiography (ICA), has been used as the yardstick for the past
33 decade or so, but it has limitations, including a substantial inter-operator interpretation
34 variability [3]–[5]. Hence, clinical practice and research has been increasingly geared toward the
35 use of the non-invasive CTA technique to express the clinical effect of plaque structure and
36 patient outcome [2]. Moreover, studies have found a link between the amount of coronary artery
37 calcification (CAC) and a robust and independent forecaster of CVD [6]. Typically, to quantify
38 the amount of calcification, two CT scans are required: a calcium scoring CT (CSCT) and a CTA
39 scan, where the CTA scan is used for the detection of non-calcified plaque and stenosis. On the
40 contrary, the amount of calcium is determined by the CSCT scan [7].
41
42
43
44
45
46
47
48
49
50

51
52 In order to decrease the radiation dose during cardiac CT exam, many studies have recently
53 focused on directly using the CTA to quantify calcium, therefore avoiding the CSCT scan [8]–
54 [10]. The manual identification of CAC in cardiac CT is tedious and time-consuming, and
55 numerous studies have been presented in the literature to semi-automatically or automatically
56 calculate calcium from CTA scanning, which typically requires an initial segmentation of the
57 coronary arteries in the imagery. CAC is then either determined as a digression from a trend line
58
59
60

1
2
3 via the lumen strength [11], [12], as voxels that present an intensity beyond a patient-specific
4 Hounsfield Unit (HU) limit within the arteries [13], or as a deviation from a model of non-
5 calcified arterial sections [14]. Recent research in this field has included the implementation of
6 deep learning techniques that automatically segment and quantify calcifications in the coronary
7 arteries [15]–[19]. In particular, Wolterink et al. [16] also provided an assessment of cardiac CT-
8 based automated coronary calcium scoring using 32 training and 40 test exams, where four
9 methods utilized both CSCT and CTA scans, while one only used CSCT. Some of the techniques
10 tested in this study provided satisfying results, showing high sensitivity (Sen), positive
11 predictive value (Ppv), and F1-score (between all methods; for details please refer to the original
12 study [16]) for CAC lesion detection equal to 94%, 96%, and 95%, respectively. However, as
13 stated previously, the majority of these techniques also relied on a CSCT scan. In another study,
14 Wolterink et al. [17] provided a solution for automatic calcium lesion detection that did not rely
15 on a CSCT scan or on coronary artery segmentation, and was based on paired convolutional
16 neural networks. In their study, the authors showed a best sensitivity for lesion identification
17 equal to 72%.

18
19
20
21
22
23
24
25
26
27
28
29
30
31
32
33 Herein, we propose a novel algorithm for the automatic detection of calcified plaque lesions
34 using only CTA scans, based upon higher order spectrum (HOS) cumulants. The method utilizes
35 image preprocessing, the Radon transform (RT), calculation of HOS cumulants, feature
36 reduction and ranking, and classification. As can be noted, the presented technique does not rely
37 on any segmentation of the coronary arteries within the CTA scan, which would limit
38 applicability in CAC identification, as severe CAC deposits affect the performance of
39 identification methods [20].

46 47 48 **2. Materials and Methods**

49 50 **2.1 Image database**

51
52 The CTA patient scans were performed with a retrospectively ECG-gated protocol, using a
53 2×32 detector row dual-source CT scanner (Siemens Somatom Definition DS, Siemens Healthcare,
54 Erlangen, Germany) at the University of Malaya Medical Centre, Department of Biomedical
55 Imaging, Malaysia. The analysis of scans acquired from the left anterior descending (LAD)
56 revealed that 30 calcified plaques and 30 normal arteries were present in the 60 patient group
57 (30 female and 30 male, age range: 39 and 81 years, mean value 61.7 ± 9.9 years). For each patient,
58
59
60

1
2
3 a total of 36 true axial views of the proximal LAD (36 mm from bifurcation of LAD and left
4 circumflex (LCx)) were generated at an interval of 1mm from the curved multi-planar
5 reformations (MPR), using a cardiac software package with cutting-edge technology (Syngo.via,
6 Siemens Healthcare, Erlangen, Germany) that is readily available for purchase by the public.
7 (Figure 1). A summary of the image database used in this study is given in Table 1.
8
9
10
11
12

13 14 2.2 Automatic calcified plaque detection algorithm

15
16 Figure 2 displays a step-by-step diagram of the detection algorithm that we propose. Firstly,
17 the image is preprocessed and the Radon transform is computed. Thereafter, the cumulant
18 features are extracted and then reduced using several techniques. Finally, a statistical analysis is
19 done and a classification is obtained using several methods.
20
21
22
23

24 25 2.2.1 Image preprocessing

26
27 Examples of the input images to the entire algorithm are shown in Figure 3 (no plaque) and
28 4 (calcified plaque). The initial step in the calcified plaque detection algorithm is image
29 preprocessing. This step is fundamental to increase the image contrast and to standardize the
30 image pixel intensity distribution. An adaptive histogram equalization algorithm [21] was
31 employed for this operation.
32
33
34
35
36

37 38 2.2.2 Radon transform (RT)

39
40 The RT is typically employed in CT to reconstruct an image from scattering data signals,
41 taking advantage of its mathematical properties, such as symmetry, scaling, linearity, shift,
42 and rotational invariance, in order to discriminate objects [22], [23]. It is also possible to
43 employ the RT to alter 2D images into lines that contain specific parameters given by the
44 projection of the image intensity along a radial line that is oriented at a specific angle. This
45 results in the generation of a line integral which is the summation of the intensities of pixels
46 studied in each direction. Being directional, the RT is thus able to capture directional features,
47 while still preserving pixel intensity variations, which aids in the preservation and boosting
48 of the spatial-frequency information contained in the image. In this work, we computed the
49 RT on every image, with a step size of 10 degrees (i.e., 0° , 10° , 20° , ..., 170°), giving forth 17
50 different 1D RT sonogram signals.
51
52
53
54
55
56
57
58
59
60

2.2.3 Higher order spectrum (HOS) cumulant feature extraction

Once the RT is applied to the image at every 10° increment, HOS cumulants are then determined for the 1D RT projections. The HOS cumulants are nonlinear combinations of higher-order moments [24]. The benefit of calculating the cumulants is that they are able to capture both the dynamic and nonlinear nature of the input signal. They can be defined as follows.

Let $x(n) = \{x_1, x_2, \dots, x_k\}$ be the k -dimensional vector of a RT CTA image. The first three moments of $x(n)$, denoted as m_{1_x}, m_{2_x} , and m_{3_x} can be defined as:

$$m_{1_x} = E[x(n)] \quad (1)$$

$$m_{2_x}(\tau_1) = E[x(n)x(n + \tau_1)] \quad (2)$$

$$m_{3_x}(\tau_1, \tau_2) = E[x(n)x(n + \tau_1)x(n + \tau_2)] \quad (3)$$

where $E[\cdot]$ is the statistical expectation operator, and τ_1 and τ_2 are the time lag parameters.

Moreover, the first three cumulants of a zero mean process, denoted as c_{1_x}, c_{2_x} , and c_{3_x} can be defined as:

$$c_{1_x} = m_{1_x} \quad (4)$$

$$c_{2_x}(\tau_1) = m_{2_x}(\tau_1) \quad (5)$$

$$c_{3_x}(\tau_1, \tau_2) = m_{3_x}(\tau_1, \tau_2) \quad (6)$$

In the system we present here, we used third-order HOS cumulants of the RT projections. The HOS cumulants that are calculated on each 1D sinogram are described using 136 features; since each image is described with 18 RT sinograms, the total number of features that are used to describe each image is therefore equal to 2448. Figure 5 shows an example of HOS cumulant plots obtained for both a CTA image containing no plaque (first row) and a CTA image containing a calcified plaque (second row).

2.2.4 Feature reduction

Due to the fact that a great number of features are used to represent each image, we tested several data reduction techniques. In particular, we employed the Kernel PCA (KPCA), Locality Preserving Projection (LPP), Locality Sensitive Discriminant Analysis (LSDA), Multiple Factor Analysis (MFA), Principal Component Analysis (PCA) and Neighborhood Preserving Embedding (NPE).

1
2
3
4
5 The LPP technique is a linear dimensionality diminution algorithm that is based on the same
6
7 variational principle that gives rise to the Laplacian Eigenmap, and therefore has similar
8
9 locality preserving properties [25]. PCA is a common statistical method to extract meaningful
10
11 features, which is unsupervised and targets to chart the data along the direction having the
12
13 highest variance [26]. The KPCA method is an extension of PCA, in which the originally
14
15 linear PCA operations are performed in a reproducing kernel Hilbert space [27]. MFA is an
16
17 extension PCA that is tailored to identify correlated structure between data sets with
18
19 matched observations [28]. The main purpose of the LSDA feature reduction technique is to
20
21 locate a projection which increases the boundary between data from different classes at each
22
23 local area [26]. The NPE is another reduction algorithm, focusing on preserving local
24
25 structure [26], [29].
26

27 2.2.5 Statistical analysis and classification

28
29 Once the features are reduced using various methods as mentioned in the previous
30
31 subsection, a statistical test is employed to identify highly significant features. In this work,
32
33 we used Student's t-test, where the features with a higher t-value will represent those that
34
35 are considered to be significant, while features with a lower t-value will be ranked as less
36
37 important. Therefore, the reduced features that have the lowest t-values will be considered
38
39 to best differentiate between images containing no plaque versus those containing a calcified
40
41 plaque.
42

43
44 The obtained ranked features were then used to enable the completely automatic
45
46 classification of images containing no plaque and those with a calcified plaque using various
47
48 classification methods. We used the following well-established techniques for this purpose:
49
50 decision tree (DT), linear discriminant analysis (LDA), quadratic discriminant analysis
51
52 (QDA), support vector machine (SVM), k-nearest neighbor (k-NN), and probabilistic neural
53
54 network (PNN). Also, the SVM classifier with polynomials 1 to 3, coupled with the radial
55
56 basis function(RBF) were employed. [30]. These classification techniques are explicitly
57
58 described by Acharya et al. [31].
59
60

3. Results

3.1 Feature extraction results

Since each image is described with 2448 features, reduction techniques were incorporated to better compare the results. Table 2 shows the utilized techniques, with the number of significant features which were obtained for each method, as determined by the Student's t-test and ranking. Regarding further detail for each feature reduction method, Table 3 shows the 12 significant features for the KPCA method. Table 4 displays the 12 significant features found using LPP; Table 5 shows the 16 found using the LSDA feature reduction method; Table 6 shows the 22 significant features determined with the MFA technique; Table 7 displays the 14 features found with NPE; finally Table 8 shows the 30 obtained reduced features using PCA. It can be noted from Table 6 that the t-values are higher using MFA than other data reduction techniques. Figure 5 shows the HOS cumulant plots of no plaque and plaque CTA images. These plots show distinctive differences for the two classes.

3.2 Classification results

In this study we employed several well-established classification techniques to process each image as either containing no plaque or containing a calcified plaque. Table 9 summarizes, for each feature reduction technique, which classification method yielded the best results in terms of accuracy, PPV, sensitivity, and specificity. As can be appreciated from the table, that the MFA feature reduction was able to obtain the best classification result among 21 features and a RBF support vector machine classifier. Specifically, a final accuracy of 95.83% was obtained, with a PPV equal to 97.05% and a sensitivity and specificity equal to 94.54% and 97.13%, respectively. To compare classification methods using the MFA feature reduction method, Table 10 shows the results obtained for all of the employed techniques. It can be appreciated that all classification methods provide satisfactory results, many being even higher than the best results obtained using a different feature reduction technique. Figure 6 shows a plot of the first two (MFA8 vs MFA2) MFA coefficients, displaying how even the first two coefficients are capable of exhibiting a distinction between a no plaque image and an image containing a calcified plaque. Hence, we have obtained the highest classification performance using MFA data reduction technique.

4. Discussion and conclusions

1
2
3 In the present study, a database comprising 2060 images from 60 patients was utilized to develop
4 an automated system for detecting the presence of a calcified plaque contained within a CTA scan,
5 and to evaluate the performance of the system. The method is based on the RT, the subsequent
6 calculation of HOS cumulants, and feature reduction and ranking using numerous well-established
7 feature reduction techniques. We showed how, among all of the employed methods, the MFA
8 feature reduction algorithm exhibited by far the best classification results using the SVM coupled
9 with a radial basis function. This algorithm is tailored to identify correlated structure between data
10 sets with matched observations, which proved fundamental in obtaining a high accuracy of 95.83%,
11 when compared to the other feature reduction methods from which was obtained a second-best
12 accuracy equal to 90.23% (LSDA). Moreover, it can be appreciated from Table 9 how, when
13 compared to the second-best performing LSDA technique, the MFA method showed an approximate
14 3 to 5% increase in both accuracy and sensitivity, and an almost 10% increase when considering PPv
15 and specificity. This demonstrates how the MFA feature reduction technique, coupled with a SVM
16 and radial basis function, is able to greatly reduce the number of false positives (i.e., images classified
17 as containing calcified plaque that do not really contain it).
18
19
20
21
22
23
24
25
26
27
28
29
30
31
32

33 As mentioned in the Introduction, the clinical setting is becoming more geared toward the use
34 of non-invasive imaging techniques for the classification and characterization of coronary
35 atherosclerotic plaques, where CTA plays a fundamental role. Since the presence of a calcified
36 plaque has been shown to have an important predictive value for the occurrence of a CVD event, it
37 is of fundamental importance to be able to automatically and accurately detect its presence [6].
38 Moreover, the use of only one CT scan (i.e., only the CTA scan and not CTA + CSCT scans) presents
39 the advantage of reducing both healthcare costs and the radiation dose a patient must be subject to
40 [32]. Various studies have been previously presented in the literature to confront the issue of
41 automatic detection of calcified plaque in CTA images. However, many of the techniques rely on a
42 first initial segmentation of the coronary artery tree, which can preclude a correct detection in the
43 case of a complex anatomy, during scans with motion or noise artefacts, coronary artery occlusions
44 or distal segments of the vessels [17]. On the other hand, many techniques are also only semi-
45 automatic, requiring an operator to interact with the system to either correct potential errors or to
46 initialize the algorithm [16]. Contrarily, Wolterink et al. [17] presented in 2016 a completely
47 automatic method using only CTA images, based on paired convolutional neural networks for the
48 detection and quantification of CAC, that did not require any initial segmentation. While the method
49
50
51
52
53
54
55
56
57
58
59
60

1
2
3 provided quantitative measurements of a calcium score that showed a good agreement with
4 reference scores, in the best-case scenario it detected only 72% of lesions in the test set (i.e., sensitivity
5 = 72%).
6
7
8
9

10 The algorithm that we developed and presented in this study has several advantages:

- 11 • A completely automatic classification of calcified plaque without using any
12 segmentation method for the coronary artery tree, or any user-interaction;
- 13 • HOS cumulants are able to extract important distinguishable features from the CTA
14 image;
- 15 • High performance results: a sensitivity, accuracy and specificity of 94.54%, 95.83%, and
16 97.13%, respectively, were obtained using an MFA feature reduction method coupled
17 with a SVM with a radial basis function;
18
19
20
21
22
23
24
25

26
27 There are also some limitations to this work. Firstly, the database only contained information
28 from 60 patients, with either no plaque or a calcified plaque. Therefore, in future work it will be
29 necessary to expand the database to include more patients, and to include images of non-calcified
30 plaques, in order to test its expanded applicability. Furthermore, the proposed method provided a
31 satisfactory sensitivity level for calcified plaque determination, but no quantitative calcium score is
32 calculated. Our future work should include the subsequent implementation of an algorithm for the
33 calculation of a quantitative calcium score on images where a calcified plaque is automatically
34 determined. Deep learning is a part of the artificial intelligence approach that eliminates feature
35 extraction, feature reduction, and categorization, incorporating the entire methodology into one
36 typically convolutional model. In the future, we plan to design a convolutional neural network
37 model with a larger database to not only detect calcified plaque, but also to automatically calculate
38 the calcium score.
39
40
41
42
43
44
45
46
47
48
49
50

51 In conclusion, this work proposes a novel approach using HOS cumulants, combined with
52 numerous feature reduction techniques, to automatically identify a calcified plaque. The system
53 exhibited promising performance results, and may be developable as a tool for assisting doctors in
54 locating calcified plaques in CTA images.
55
56
57
58
59
60

Acknowledgement

1
2
3 We thank the radiologists and radiographers at the University of Malaya Medical Centre for their
4 kind assistance.
5
6
7

8 9 **Funding**

10 This study was supported by the High Impact Research Chancellery Grant
11 UM.C/625/1/HIR/MOHE/MED/36 from the Ministry of Education, Malaysia, and the Postgraduate
12 Research Grant PG307-2016A from the University of Malaya, Malaysia.
13
14
15
16
17

18 **Conflict of interest:**

19 None
20
21
22

23 **Ethic approval**

24 Medical Ethics Committee of the University of Malaya Medical Centre (Protocol no: 989.35)
25
26
27
28

29 **References**

- 30 [1] Agoston-Coldea, L., Cionca, C. & Lupu, S. (2005). Coronary CT Angiography and the
31 Napkin-ring Sign Indicates High-Risk Atherosclerotic Lesions. *Intech open*.
32
33 [2] Sato, A. (2014). Coronary plaque imaging by coronary computed tomography angiography.
34 *World Journal of Radiology*, 6(5), 148.
35
36 [3] White, C.W., Wright, C.B., Doty, D.B., Hiratza, L.F., Eastham, C.L., Harrison, D.G., Marcus,
37 M.L. (1984). Does Visual Interpretation of the Coronary Arteriogram Predict the Physiologic
38 Importance of a Coronary Stenosis? *The New England Journal of Medicine*, 310(13), 819–824.
39
40 [4] Marcus, M.L., Harrison, D.G., White, C.W., McPherson, D.D., Wilson, R.F., & Kerber,
41 R.E. (1988). Assessing the physiologic significance of coronary obstructions in patients:
42 Importance of diffuse undetected atherosclerosis. *Progress in Cardiovascular Diseases*, 31(1),
43 39–56.
44
45 [5] Vogel, R.A. (1988). Assessing Stenosis Significance by Coronary Arteriography: Are the Best
46 Variables Good Enough?
47
48 [6] Yeboah, J et al (2012). Comparison of Novel Risk Markers for Improvement in
49 Cardiovascular Risk Assessment in Intermediate-Risk Individuals, *Journal of the American*
50 *Medical Association*, 38(8), 788-795.
51
52 [7] Hecht, H.S. (2015), Coronary Artery Calcium Scanning: Past, Present, and Future, *Journal of*
53
54
55
56
57
58
59
60

1
2
3
4
5
6
7
8
9
10
11
12
13
14
15
16
17
18
19
20
21
22
23
24
25
26
27
28
29
30
31
32
33
34
35
36
37
38
39
40
41
42
43
44
45
46
47
48
49
50
51
52
53
54
55
56
57
58
59
60

the American College of Cardiology: Cardiovascular Imaging, 8(5), 579–596.

- [8] Pavitt, C.W et al (2014). Deriving coronary artery calcium scores from CT coronary angiography: a proposed algorithm for evaluating stable chest pain, *The International Journal of Cardiovascular Imaging*, 30(6), 1135–1143.
- [9] Messenger, B., Li, D., Nasir, K., Carr, J.J., Blankstein, R., & Budoff, M.J. (2016). Coronary calcium scans and radiation exposure in the multi-ethnic study of atherosclerosis, *International Journal of Cardiovascular Imaging*, 32(3), 525–529.
- [10] Al-Mallah, M.H., Aljizeeri, A., Alharthi, M., & Alsaileek, A. (2014). Routine low-radiation-dose coronary computed tomography angiography, *European Heart Journal Supplements*, 16(supplement B), B12–B16.
- [11] Wesarg, S., Khan, M.F., & Firle, E.A. (2006). Localizing Calcifications in Cardiac CT Data Sets Using a New Vessel Segmentation Approach, *Journal of Digital Imaging*, 19(3), 249–257.
- [12] Ahmed, W et al (2015). Automatic detection and quantification of the Agatston coronary artery calcium score on contrast computed tomography angiography, *International Journal of Cardiovascular Imaging*, 31(1), 151–161.
- [13] Teßmann, M., Vega-Higuera, F., Bischoff, B., Hausleiter, J., & Greiner, G. (2011). Automatic detection and quantification of coronary calcium on 3D CT angiography data, *Computer Science Research and Development*, 26(1-2), 117–124.
- [14] Eilat, D. & Goldenberg, R. (2014). Fully automatic model-based calcium segmentation and scoring in coronary CT angiography, *International Journal of Computer Assisted Radiology and Surgery*, 9(4), 595–608.
- [15] Zreik, M., van Hamersvelt, R.W., Wolterink, J.M., Leiner, T., Viergever, M.A., & Išgum, I. (2019). A Recurrent CNN for Automatic Detection and Classification of Coronary Artery Plaque and Stenosis in Coronary CT Angiography, *IEEE Transactions on Medical Imaging*.
- [16] Wolterink, J.M et al (2016). An evaluation of automatic coronary artery calcium scoring methods with cardiac CT using the orCaScore framework, *Medical Physics*, 43(5) 2361–2373.
- [17] Wolterink, J.M., Leiner, T., de Vos, B.D., van Hamersvelt, R.W., Viergever, M.A., & Išgum, I. (2016). Automatic coronary artery calcium scoring in cardiac CT angiography using paired convolutional neural networks, *Medical Image Analysis*, 34, 123–136.
- [18] Lessmann, N et al (2018). Automatic Calcium Scoring in Low-Dose Chest CT Using Deep Neural Networks With Dilated Convolutions, *IEEE Transactions on Medical Imaging*, 37(2), 615–625.

- 1
2
3 [19] Shadmi, R., Mazo, V., Bregman-Amitai, O., & Elnekave, E.(2018). Fully-convolutional deep-
4 learning based system for coronary calcium score prediction from non-contrast chest CT,
5 2018 IEEE 15th International Symposium on Biomedical Imaging (ISBI 2018), 24-28.
6
7
8 [20] Schaap, M et al (2009). Standardized evaluation methodology and reference database for
9 evaluating coronary artery centerline extraction algorithms," *Medical Image Analysis*, 13(5),
10 701–714.
11
12
13 [21] Pizer, S.M et al (1987). Adaptive histogram equalization and its variations," *Computer Vision,*
14 *Graphics and Image Processing*, 39(3),355–368.
15
16
17 [22] Mookiah, M.R.K et al (2015). Application of higher-order spectra for automated grading of
18 diabetic maculopathy," *Medical and Biological Engineering and Computing*, 53(12),1319–1331.
19
20
21 [23] Radon, J.(1986). On the determination of functions from their integral values along certain
22 manifolds, *IEEE Transactionas on Medical Imaging*, 5(4), 170–176.
23
24
25 [24] Noronha, K.P., Acharya, U.R., Nayak, k.P., Martis, R.J., & Bhandary, S.V.(2014). Automated
26 classification of glaucoma stages using higher order cumulant features, *Biomedical Signal*
27 *Processing Control*, 10(1), 174–183.
28
29
30 [25] He, X., Niyogi, P.(2004) in neural information processing systems, and undefined 2004,
31 Locality preserving projections, *Advances in. Neural Information Processing Systems*, 153–160.
32
33
34 [26] Cai, D., He, X., Zhou, K., Han, J., & Bao, H.(2007). Locality Sensitive Discriminant Analysis
35 in *20th International Joint Conference on Artificial Intelligence*, 708–713.
36
37
38 [27] Schölkopf, B., Smola, A., & Müller, K.R.(1988). Nonlinear Component Analysis as a Kernel
39 Eigenvalue Problem, *Neural Computation*, 10(5), 1299–1319.
40
41
42 [28] Meng, C., Zeleznik, O.A.,Thallinger, G.G., Kuster, B., Gholami, A.M., & Culhane, A.C.(2016).
43 Dimension reduction techniques for the integrative analysis of multi-omics data," *Briefings*
44 *in Bioinformatics*, 17(4), 628–641.
45
46
47 [29] He, X., Cai, D., Yan, S., & Zhang, H.J(2005). Neighborhood preserving embedding in *Tenth*
48 *IEEE International Conference on Computer Vision (ICCV'05)*,1, 1208–1213.
49
50
51 [30] Duda, R., Hart, P., & Stork, D.(2012). *Pattern classification*.
52
53
54 [31] U. R. Acharya et al(2016). Automated characterization of fatty liver disease and cirrhosis
55 using curvelet transform and entropy features extracted from ultrasound images, *Computers*
56 *in Biology and Medicine*, 79, 250–258.
57
58
59 [32] Voros, S., & Qian, Z.(2012). Agatston score tried and true: By contrast, can we quantify
60 calcium on CTA? *Journal of Cardiovascular Computer Tomography*, 16(1),45–47.

1
2
3
4
5
6
7
8
9
10
11
12
13
14
15
16
17
18
19
20
21
22
23
24
25
26
27
28
29
30
31
32
33
34
35
36
37
38
39
40
41
42
43
44
45
46
47
48
49
50
51
52
53
54
55
56
57
58
59
60

For Peer Review

1
2
3 **Tables and Figures**
4
5
6

7 **Table 1. Summary of patient and image database.**
8
9

10 **Table 2. Summary of feature reduction methods employed.**
11

12 KPCA: Kernel PCA;

13 LPP: Locality Preserving Projection;

14 LSDA: Locality Sensitive Discriminant Analysis;

15 MFA: Multiple Factor Analysis;

16 PCA: Principal Component Analysis;

17 NPE: Neighborhood Preserving Embedding
18
19
20
21
22
23
24
25
26
27
28
29
30
31
32
33
34
35
36
37
38
39
40
41
42
43
44
45
46
47
48
49
50
51
52
53
54
55
56
57
58
59
60

For Peer Review

1
2
3
4
5
6
7
8
9
10
11
12
13
14
15
16
17
18
19
20
21
22
23
24
25
26
27
28
29
30
31
32
33
34
35
36
37
38
39
40
41
42
43
44
45
46
47
48
49
50
51
52
53
54
55
56
57
58
59
60

Table 3. Results obtained after feature reduction using Kernel Principal Component Analysis (KPCA).

Table 4. Results obtained after feature reduction using Locality Preserving Projection (LPP).

Table 5. Results obtained after feature reduction using Locality Sensitive Discriminant Analysis (LSDA).

For Peer Review

1
2
3
4
5 **Table 6. Results obtained after feature reduction using Multiple Factor Analysis (MFA).**
6
7
8
9
10
11
12
13
14
15
16
17
18
19
20
21
22
23
24
25
26
27
28
29
30
31
32
33
34
35
36
37
38
39
40
41
42
43
44
45
46
47
48
49
50
51
52
53
54
55
56
57
58
59
60

For Peer Review

1
2
3
4
5
6
7
8
9
10
11
12
13
14
15
16
17
18
19
20
21
22
23
24
25
26
27
28
29
30
31
32
33
34
35
36
37
38
39
40
41
42
43
44
45
46
47
48
49
50
51
52
53
54
55
56
57
58
59
60

Table 7. Results obtained after feature reduction using Neighbourhood Preserving Embedding (NPE).

For Peer Review

1
2
3 **Table 8. Results obtained after feature reduction using Principal Component Analysis (PCA).**
4
5
6
7

8 **Table 9. Best classification results for calcification plaque determination using different feature reduction**
9 **techniques.**

10
11 para: parameters, Aç.: accuracy, PPv: positive predictive value, Sen: sensitivity, Spe: specificity
12
13
14
15

16 **Table 10. Results for the classification of calcified plaque detection using Multiple Factor Analysis (MFA)**
17 **feature reduction.**

18
19
20
21 para: parameters, Aç.: accuracy, PPv: positive predictive value, Sen: sensitivity, Spe: specificity
22
23
24
25
26
27
28
29

30 Figure 1. Curved multi-planar reformations (MPR) of the left anterior descending (LAD) artery with
31 true axial views generated at an interval of 1mm.
32
33
34
35
36
37
38
39
40
41
42

43 Figure 2. Step-by-step diagram of the calcified plaque detection algorithm.
44
45

46 Figure 3. Example CTA images with no plaque.
47
48
49
50

51
52 Figure 4. Example CTA images with calcified plaque.
53
54
55
56
57
58
59
60

1
2
3
4
5
6
7
8
9
10
11
12
13
14
15
16
17
18
19
20
21
22
23
24
25
26
27
28
29
30
31
32
33
34
35
36
37
38
39
40
41
42
43
44
45
46
47
48
49
50
51
52
53
54
55
56
57
58
59
60

Figure 5. Examples of higher order spectrum cumulants. (A) Example no plaque CTA image; (B) Contour plot of no plaque CTA image; (C) 3D contour plot of no plaque CTA image; (D) Example calcified plaque CTA image; (E) Contour plot of calcified plaque CTA image; (F) 3D contour plot of calcified plaque CTA image.

Figure 6. Scatter plot showing first two MFA features of non-calcified plaque in blue, and calcified plaques in red color.

For Peer Review

1
2
3
4
5
6
7
8
9
10
11
12
13
14
15
16
17
18
19
20
21
22
23
24
25
26
27
28
29
30
31
32
33
34
35
36
37
38
39
40
41
42
43
44
45
46
47
48
49
50
51
52
53
54
55
56
57
58
59
60

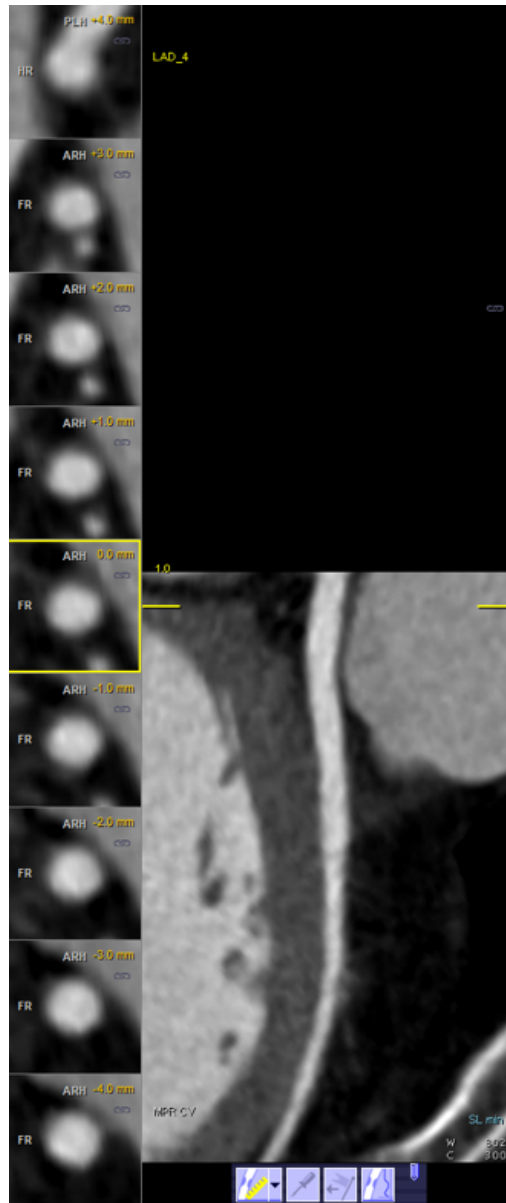


Figure 1. Curved multi-planar reformations (MPR) of the left anterior descending (LAD) artery with true axial views generated at an interval of 1mm.

1
2
3
4
5
6
7
8
9
10
11
12
13
14
15
16
17
18
19
20
21
22
23
24
25
26
27
28
29
30
31
32
33
34
35
36
37
38
39
40
41
42
43
44
45
46
47
48
49
50
51
52
53
54
55
56
57
58
59
60

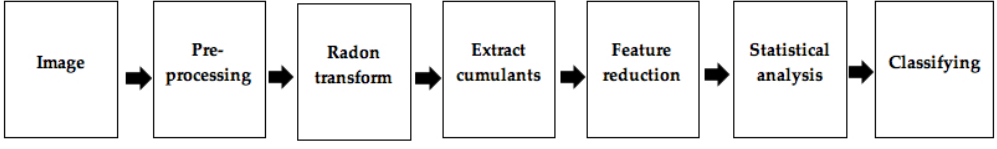


Figure 2. Step-by-step diagram of the calcified plaque detection algorithm.

283x43mm (72 x 72 DPI)

1
2
3
4
5
6
7
8
9
10
11
12
13
14
15
16
17
18
19
20
21
22
23
24
25
26
27
28
29
30
31
32
33
34
35
36
37
38
39
40
41
42
43
44
45
46
47
48
49
50
51
52
53
54
55
56
57
58
59
60

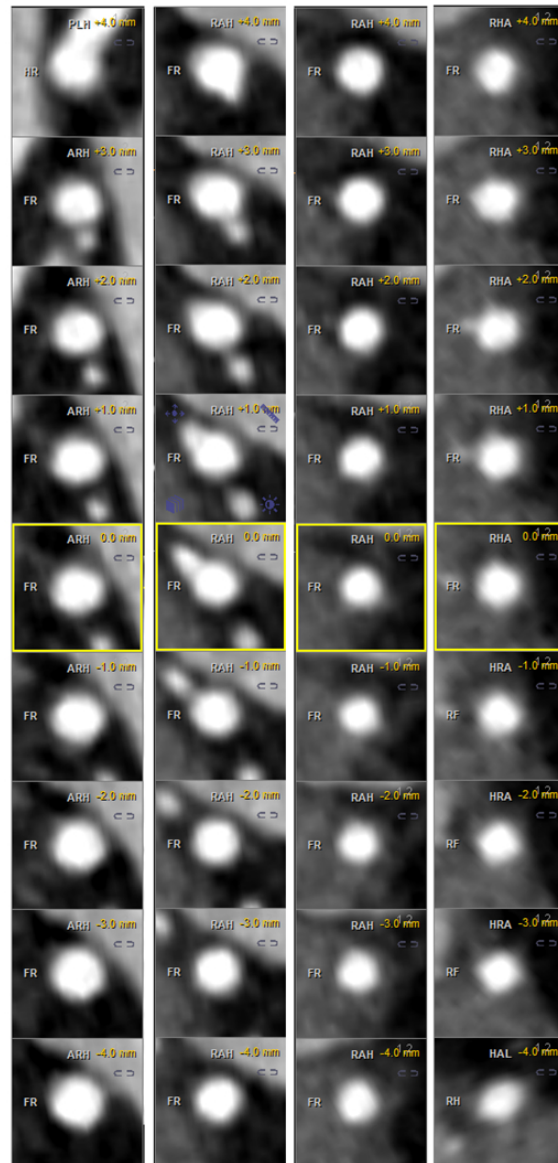


Figure 3. Example CTA images with no plaque.

1
2
3
4
5
6
7
8
9
10
11
12
13
14
15
16
17
18
19
20
21
22
23
24
25
26
27
28
29
30
31
32
33
34
35
36
37
38
39
40
41
42
43
44
45
46
47
48
49
50
51
52
53
54
55
56
57
58
59
60

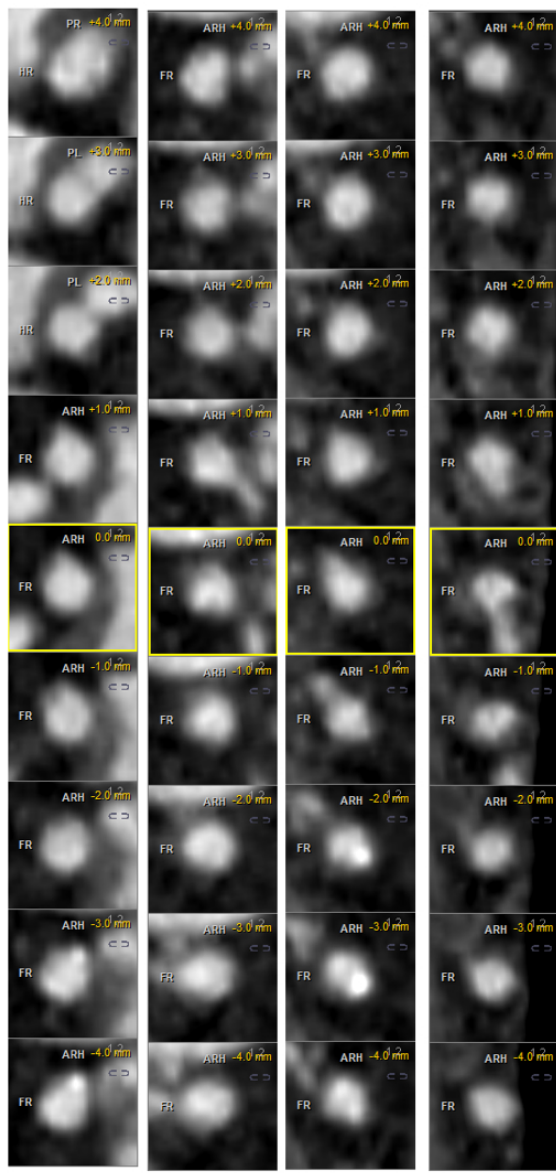


Figure 4. Example CTA images with calcified plaque.

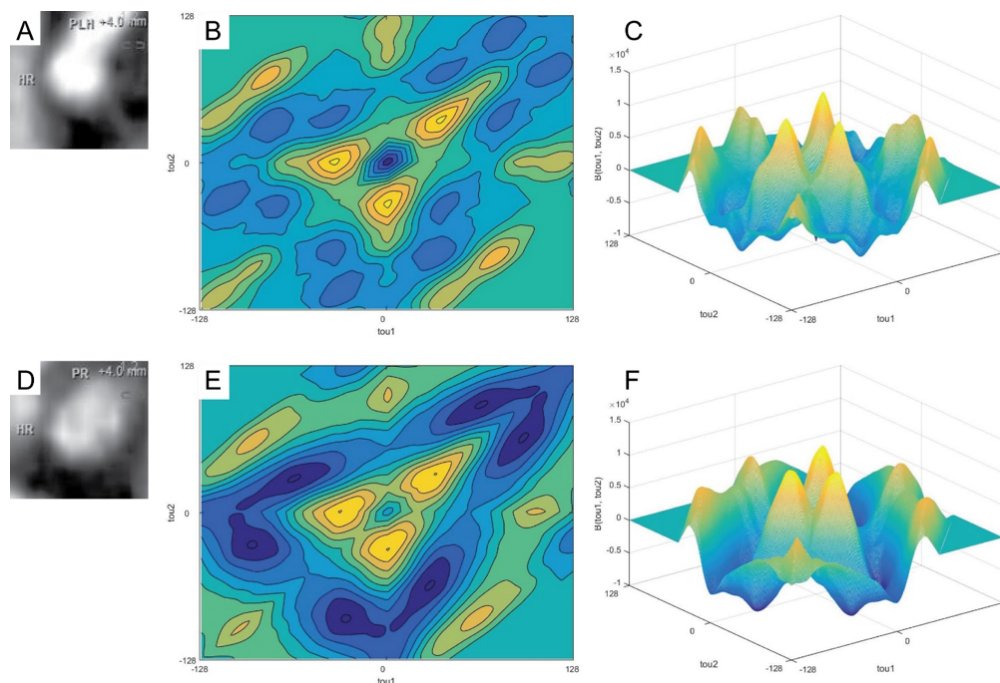


Figure 5. Examples of higher order spectrum cumulants. (A) Example no plaque CTA image; (B) Contour plot of no plaque CTA image; (C) 3D contour plot of no plaque CTA image; (D) Example calcified plaque CTA image; (E) Contour plot of calcified plaque CTA image; (F) 3D contour plot of calcified plaque CTA image.

1
2
3
4
5
6
7
8
9
10
11
12
13
14
15
16
17
18
19
20
21
22
23
24
25
26
27
28
29
30
31
32
33
34
35
36
37
38
39
40
41
42
43
44
45
46
47
48
49
50
51
52
53
54
55
56
57
58
59
60

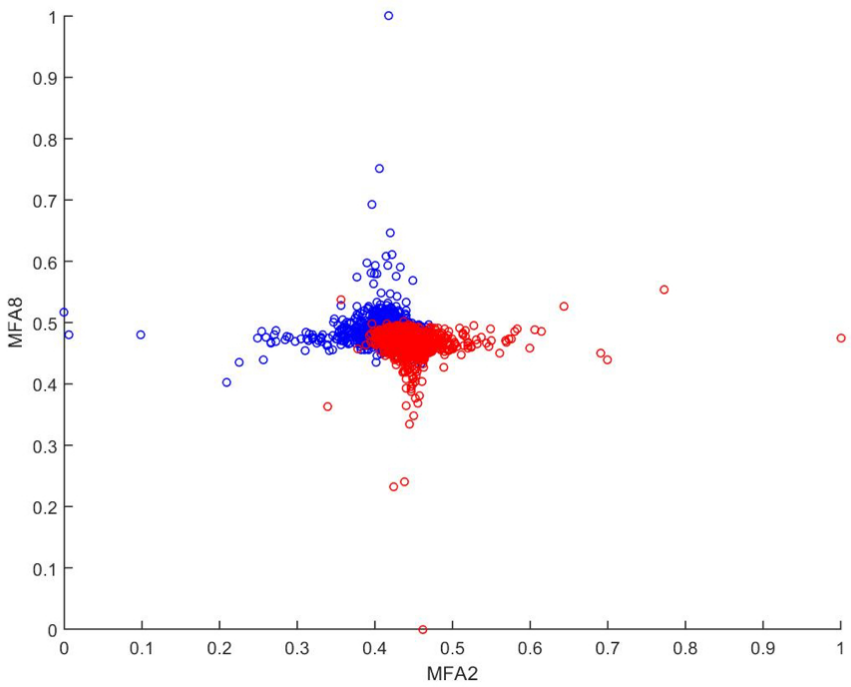


Figure 6. Scatter plot showing first two MFA features of non-calcified plaque in blue, and calcified plaques in red color.

Table 1. Summary of patient and image database.

| Class | Number of subjects | Number of images |
|------------------|--------------------|------------------|
| No plaque | 30 | 1080 |
| Calcified plaque | 30 | 1080 |

Table 2. Summary of feature reduction methods employed.

| Algorithm | Total number of features | Number of significant features |
|-----------|--------------------------|--------------------------------|
| KPCA | 30 | 12 |
| LPP | 30 | 12 |
| LSDA | 30 | 16 |
| MFA | 30 | 22 |
| NPE | 30 | 14 |
| PCA | 435 | 30 |

Table 3. Results obtained after feature reduction using Kernel Principal Component Analysis (KPCA).

| kPCA coefficient | No plaque | | Calcified plaque | | p-value | t-value |
|------------------|-----------|--------|------------------|--------|---------|---------|
| | Mean | SD | Mean | SD | | |
| kPCA12 | 0.5410 | 0.0898 | 0.5145 | 0.1084 | 0.0000 | 6.1853 |
| kPCA23 | 0.4889 | 0.1085 | 0.4692 | 0.1211 | 0.0001 | 3.9873 |
| kPCA17 | 0.4663 | 0.0797 | 0.4786 | 0.0858 | 0.0006 | 3.4562 |
| kPCA28 | 0.4700 | 0.0553 | 0.4781 | 0.0602 | 0.0011 | 3.2768 |
| kPCA7 | 0.4872 | 0.0891 | 0.4741 | 0.1004 | 0.0014 | 3.2052 |
| kPCA5 | 0.5115 | 0.0742 | 0.5210 | 0.0824 | 0.0047 | 2.8294 |

| | | | | | | |
|---------------|--------|--------|--------|--------|--------|--------|
| kPCA4 | 0.5975 | 0.0722 | 0.5885 | 0.0867 | 0.0088 | 2.6227 |
| kPCA29 | 0.5982 | 0.1040 | 0.5867 | 0.1070 | 0.0116 | 2.5274 |
| kPCA3 | 0.7970 | 0.0780 | 0.7889 | 0.0781 | 0.0162 | 2.4067 |
| kPCA11 | 0.6414 | 0.0673 | 0.6486 | 0.0820 | 0.0241 | 2.2571 |
| kPCA21 | 0.5104 | 0.0987 | 0.5200 | 0.1113 | 0.0326 | 2.1379 |
| kPCA15 | 0.5065 | 0.0767 | 0.4995 | 0.0891 | 0.0493 | 1.9673 |

Table 4. Results obtained after feature reduction using Locality Preserving Projection (LPP).

| LPP coefficient | No plaque | | Calcified plaque | | p-value | t-value |
|--------------------|-----------|--------|------------------|--------|---------|---------|
| | Mean | SD | Mean | SD | | |
| LPP13 | 0.3839 | 0.0748 | 0.4062 | 0.0916 | 0.0000 | 6.2174 |
| LPP9 | 0.5786 | 0.0943 | 0.5546 | 0.1100 | 0.0000 | 5.4452 |
| LPP26 | 0.5884 | 0.0622 | 0.5714 | 0.0845 | 0.0000 | 5.2979 |
| LPP10 | 0.6216 | 0.0572 | 0.6104 | 0.0680 | 0.0000 | 4.1662 |
| LPP17 | 0.5067 | 0.1067 | 0.4893 | 0.1045 | 0.0001 | 3.8349 |
| LPP18 | 0.4814 | 0.0849 | 0.4673 | 0.0966 | 0.0003 | 3.6030 |
| LPP5 | 0.4138 | 0.0647 | 0.4027 | 0.0858 | 0.0007 | 3.3953 |
| LPP7 | 0.7195 | 0.0897 | 0.7327 | 0.0901 | 0.0007 | 3.3900 |
| LPP12 | 0.6169 | 0.0662 | 0.6272 | 0.0760 | 0.0008 | 3.3626 |
| LPP29 | 0.3352 | 0.0802 | 0.3240 | 0.0796 | 0.0012 | 3.2371 |
| LPP4 | 0.4125 | 0.0819 | 0.4239 | 0.0988 | 0.0035 | 2.9277 |
| LPP21 | 0.5449 | 0.1040 | 0.5582 | 0.1123 | 0.0042 | 2.8665 |

Table 5. Results obtained after feature reduction using Locality Sensitive Discriminant Analysis (LSDA).

| LSDA coefficient | No plaque | | Calcified plaque | | p-value | t-value |
|---------------------|-----------|--------|------------------|--------|---------|---------|
| | Mean | SD | Mean | SD | | |
| LSDA9 | 0.5435 | 0.0691 | 0.5039 | 0.1116 | 0.0000 | 9.8969 |
| LSDA6 | 0.6766 | 0.0557 | 0.6467 | 0.0979 | 0.0000 | 8.7180 |
| LSDA11 | 0.5996 | 0.1102 | 0.5607 | 0.0991 | 0.0000 | 8.6189 |
| LSDA8 | 0.4978 | 0.0663 | 0.4723 | 0.0734 | 0.0000 | 8.4847 |
| LSDA4 | 0.2318 | 0.0638 | 0.2602 | 0.0920 | 0.0000 | 8.3225 |
| LSDA14 | 0.5254 | 0.1019 | 0.5603 | 0.1019 | 0.0000 | 7.9602 |
| LSDA21 | 0.6342 | 0.0575 | 0.6137 | 0.0806 | 0.0000 | 6.8070 |
| LSDA12 | 0.8278 | 0.0440 | 0.8132 | 0.0635 | 0.0000 | 6.2001 |
| LSDA20 | 0.6289 | 0.0791 | 0.6486 | 0.1045 | 0.0000 | 4.9544 |
| LSDA17 | 0.6518 | 0.0879 | 0.6326 | 0.0990 | 0.0000 | 4.7539 |
| LSDA15 | 0.4543 | 0.0827 | 0.4382 | 0.0805 | 0.0000 | 4.5812 |
| LSDA26 | 0.5382 | 0.0839 | 0.5546 | 0.0866 | 0.0000 | 4.4499 |
| LSDA3 | 0.7363 | 0.1265 | 0.7162 | 0.1434 | 0.0006 | 3.4536 |
| LSDA16 | 0.5768 | 0.1045 | 0.5617 | 0.1076 | 0.0009 | 3.3103 |
| LSDA7 | 0.4854 | 0.0877 | 0.4727 | 0.0967 | 0.0015 | 3.1847 |
| LSDA19 | 0.5413 | 0.0947 | 0.5297 | 0.0972 | 0.0050 | 2.8075 |

Table 6. Results obtained after feature reduction using Multiple Factor Analysis (MFA).

| MFA coefficient | No plaque | | Calcified plaque | | p-value | t-value |
|--------------------|-----------|--------|------------------|--------|---------|---------|
| | Mean | SD | Mean | SD | | |
| MFA2 | 0.4099 | 0.0355 | 0.4449 | 0.0353 | 0.0000 | 22.9956 |
| MFA8 | 0.4870 | 0.0267 | 0.4657 | 0.0247 | 0.0000 | 19.3028 |
| MFA7 | 0.5206 | 0.0360 | 0.4969 | 0.0345 | 0.0000 | 15.6184 |
| MFA5 | 0.5082 | 0.0271 | 0.4933 | 0.0249 | 0.0000 | 13.3261 |
| MFA1 | 0.3775 | 0.0250 | 0.3952 | 0.0390 | 0.0000 | 12.5085 |
| MFA13 | 0.5304 | 0.0240 | 0.5185 | 0.0240 | 0.0000 | 11.5565 |
| MFA10 | 0.4975 | 0.0299 | 0.5092 | 0.0301 | 0.0000 | 9.0257 |
| MFA21 | 0.4875 | 0.1504 | 0.5375 | 0.1274 | 0.0000 | 8.3350 |
| MFA29 | 0.5333 | 0.1221 | 0.5766 | 0.1259 | 0.0000 | 8.1189 |
| MFA3 | 0.5959 | 0.0362 | 0.6074 | 0.0322 | 0.0000 | 7.7910 |
| MFA4 | 0.3739 | 0.0273 | 0.3814 | 0.0283 | 0.0000 | 6.2558 |
| MFA6 | 0.5222 | 0.0454 | 0.5330 | 0.0426 | 0.0000 | 5.7051 |
| MFA11 | 0.5700 | 0.0341 | 0.5623 | 0.0326 | 0.0000 | 5.3125 |
| MFA30 | 0.4721 | 0.1434 | 0.4425 | 0.1151 | 0.0000 | 5.3026 |
| MFA25 | 0.4751 | 0.1396 | 0.5034 | 0.1213 | 0.0000 | 5.0377 |
| MFA18 | 0.6229 | 0.0267 | 0.6187 | 0.0194 | 0.0000 | 4.1465 |
| MFA12 | 0.5178 | 0.0220 | 0.5140 | 0.0219 | 0.0000 | 4.1013 |
| MFA15 | 0.5490 | 0.0256 | 0.5455 | 0.0232 | 0.0008 | 3.3646 |
| MFA16 | 0.5350 | 0.0232 | 0.5332 | 0.0060 | 0.0139 | 2.4624 |
| MFA17 | 0.4856 | 0.0243 | 0.4838 | 0.0086 | 0.0224 | 2.2862 |

| | | | | | | |
|--------------|--------|--------|--------|--------|--------|--------|
| MFA14 | 0.6589 | 0.0300 | 0.6565 | 0.0217 | 0.0339 | 2.1223 |
| MFA26 | 0.4957 | 0.1310 | 0.5069 | 0.1202 | 0.0386 | 2.0701 |

Table 7. Results obtained after feature reduction using Neighbourhood Preserving Embedding (NPE).

| NPE coefficient | No plaque | | Calcified plaque | | p-value | t-value |
|-----------------|-----------|--------|------------------|--------|---------|---------|
| | Mean | SD | Mean | SD | | |
| NPE26 | 0.5328 | 0.0822 | 0.5583 | 0.0963 | 0.0000 | 6.6265 |
| NPE18 | 0.5368 | 0.0773 | 0.5535 | 0.0803 | 0.0000 | 4.9382 |
| NPE12 | 0.5610 | 0.0679 | 0.5729 | 0.0684 | 0.0001 | 4.0638 |
| NPE10 | 0.5757 | 0.0471 | 0.5847 | 0.0636 | 0.0002 | 3.7667 |
| NPE23 | 0.3437 | 0.0836 | 0.3570 | 0.0960 | 0.0006 | 3.4230 |
| NPE5 | 0.4012 | 0.0671 | 0.3906 | 0.0815 | 0.0009 | 3.3162 |
| NPE4 | 0.4548 | 0.0751 | 0.4663 | 0.0890 | 0.0012 | 3.2534 |
| NPE22 | 0.4347 | 0.0592 | 0.4250 | 0.0807 | 0.0015 | 3.1851 |
| NPE7 | 0.2433 | 0.0486 | 0.2531 | 0.0925 | 0.0020 | 3.0896 |
| NPE24 | 0.4185 | 0.0697 | 0.4095 | 0.0653 | 0.0020 | 3.0885 |
| NPE3 | 0.8518 | 0.0706 | 0.8419 | 0.0817 | 0.0028 | 2.9954 |
| NPE13 | 0.4326 | 0.0366 | 0.4395 | 0.0690 | 0.0037 | 2.9043 |
| NPE28 | 0.4938 | 0.0838 | 0.5054 | 0.1038 | 0.0043 | 2.8597 |
| NPE14 | 0.4826 | 0.0446 | 0.4776 | 0.0601 | 0.0268 | 2.2156 |

Table 8. Results obtained after feature reduction using Principal Component Analysis (PCA).

| PCA coefficient | No plaque | | Calcified plaque | | p-value | t-value |
|-----------------|-----------|--------|------------------|--------|---------|---------|
| | Mean | SD | Mean | SD | | |
| PCA12 | 0.5410 | 0.0898 | 0.5145 | 0.1084 | 0.0000 | 6.1853 |
| PCA68 | 0.4060 | 0.0883 | 0.4301 | 0.1038 | 0.0000 | 5.8140 |
| PCA64 | 0.4487 | 0.0927 | 0.4707 | 0.1023 | 0.0000 | 5.2286 |
| PCA106 | 0.5132 | 0.1044 | 0.4910 | 0.1111 | 0.0000 | 4.7896 |
| PCA237 | 0.5099 | 0.1130 | 0.5330 | 0.1297 | 0.0000 | 4.4080 |
| PCA179 | 0.5047 | 0.1103 | 0.5250 | 0.1163 | 0.0000 | 4.1782 |
| PCA23 | 0.5111 | 0.1085 | 0.5308 | 0.1211 | 0.0001 | 3.9873 |
| PCA107 | 0.5840 | 0.0973 | 0.5662 | 0.1133 | 0.0001 | 3.9165 |
| PCA265 | 0.4726 | 0.1070 | 0.4544 | 0.1092 | 0.0001 | 3.9123 |
| PCA188 | 0.4768 | 0.1251 | 0.4562 | 0.1332 | 0.0002 | 3.7012 |
| PCA327 | 0.5086 | 0.1333 | 0.4866 | 0.1437 | 0.0002 | 3.6884 |
| PCA105 | 0.5240 | 0.1037 | 0.5067 | 0.1187 | 0.0003 | 3.6125 |
| PCA97 | 0.5268 | 0.1038 | 0.5440 | 0.1181 | 0.0003 | 3.5999 |
| PCA17 | 0.4663 | 0.0797 | 0.4786 | 0.0858 | 0.0006 | 3.4562 |
| PCA28 | 0.4700 | 0.0553 | 0.4781 | 0.0602 | 0.0011 | 3.2768 |
| PCA7 | 0.5128 | 0.0891 | 0.5259 | 0.1004 | 0.0014 | 3.2052 |
| PCA341 | 0.5262 | 0.0911 | 0.5131 | 0.1000 | 0.0014 | 3.1984 |
| PCA180 | 0.3736 | 0.0805 | 0.3848 | 0.0831 | 0.0015 | 3.1825 |
| PCA331 | 0.4798 | 0.1102 | 0.4955 | 0.1191 | 0.0015 | 3.1752 |
| PCA45 | 0.4313 | 0.0850 | 0.4434 | 0.0943 | 0.0018 | 3.1290 |
| PCA35 | 0.6098 | 0.1011 | 0.5963 | 0.1036 | 0.0022 | 3.0627 |

| | | | | | | |
|--------|--------|--------|--------|--------|--------|--------|
| PCA65 | 0.5923 | 0.0761 | 0.5812 | 0.0934 | 0.0026 | 3.0176 |
| PCA171 | 0.5152 | 0.1008 | 0.5016 | 0.1089 | 0.0026 | 3.0158 |
| PCA242 | 0.6059 | 0.1132 | 0.6207 | 0.1184 | 0.0030 | 2.9687 |
| PCA135 | 0.5400 | 0.1038 | 0.5266 | 0.1083 | 0.0036 | 2.9181 |
| PCA170 | 0.3969 | 0.1013 | 0.4095 | 0.1017 | 0.0038 | 2.8989 |
| PCA221 | 0.5377 | 0.1043 | 0.5240 | 0.1181 | 0.0046 | 2.8387 |
| PCA292 | 0.5316 | 0.1320 | 0.5152 | 0.1371 | 0.0046 | 2.8335 |
| PCA5 | 0.5115 | 0.0742 | 0.5210 | 0.0824 | 0.0047 | 2.8294 |
| PCA44 | 0.4916 | 0.1122 | 0.4777 | 0.1168 | 0.0050 | 2.8110 |

Table 9. Best classification results for calcification plaque determination using different feature reduction techniques.

| Feature reduction technique | Classifier | No. of para. | Aç. (%) | PPv. (%) | Sen. (%) | Spe. (%) |
|-----------------------------|------------|--------------|---------|----------|----------|----------|
| KPCA | PNN | 12 | 71.62 | 75.19 | 64.54 | 78.70 |
| LPP | PNN | 19 | 76.76 | 76.04 | 78.15 | 75.37 |
| LSDA | PNN | 21 | 90.23 | 89.04 | 91.76 | 88.70 |
| MFA | SVM RBF | 21 | 95.83 | 97.05 | 94.54 | 97.13 |
| NPE | PNN | 14 | 74.86 | 75.69 | 73.24 | 76.48 |
| PCA | SVM Poly 3 | 79 | 80.56 | 81.13 | 79.63 | 81.48 |

para: parameters, Aç.: accuracy, PPv: positive predictive value, Sen: sensitivity, Spe: specificity

Table 10. Results for the classification of calcified plaque detection using Multiple Factor Analysis (MFA) feature reduction.

| Classifier | No. of para. | Aç. (%) | PPv. (%) | Sen. (%) | Spe. (%) |
|----------------|--------------|--------------|--------------|--------------|--------------|
| DT | 15 | 86.53 | 86.56 | 86.48 | 86.57 |
| LDA | 16 | 90.09 | 89.87 | 90.37 | 89.81 |
| QDA | 15 | 89.40 | 89.51 | 89.26 | 89.54 |
| SVM Poly 1 | 19 | 90.42 | 90.91 | 89.81 | 91.02 |
| SVM Poly 2 | 17 | 92.64 | 92.84 | 92.41 | 92.87 |
| SVM Poly 3 | 11 | 89.35 | 88.71 | 90.19 | 88.52 |
| k-NN | 7 | 91.39 | 90.64 | 92.31 | 90.46 |
| PNN | 7 | 91.53 | 90.66 | 92.59 | 90.46 |
| SVM RBF | 21 | 95.83 | 97.05 | 94.54 | 97.13 |

para: parameters, Aç.: accuracy, PPv: positive predictive value, Sen: sensitivity, Spe: specificity